Cancer Research

MDM2 Derived from Dedifferentiated Liposarcoma Extracellular Vesicles Induces MMP2 Production from Preadipocytes

Lucia Casadei[1,2], Federica Calore[3], Danielle A. Braggio[1,2], Abeba Zewdu[1,2], Ameya A. Deshmukh[1,4], Paolo Fadda[3], Gonzalo Lopez[1,2], Martin Wabitsch[5], Chi Song[6], Jennifer L. Leight[1,4], Valerie P. Grignol[1,2], Dina Lev[7], Carlo M. Croce[3], and Raphael E. Pollock[2]

Abstract

Dedifferentiated liposarcoma (DDLPS) is frequently diagnosed late, and patients typically respond poorly to treatments. DDLPS is molecularly characterized by wild-type p53 and amplification of the *MDM2* gene, which results in overexpression of MDM2 protein, a key oncogenic process in DDLPS. In this study, we demonstrate that extracellular vesicles derived from patients with DDLPS or from DDLPS cell lines are carriers of MDM2 DNA that can be transferred to preadipocytes, a major and ubiquitous cellular component of the DDLPS tumor microenvironment, leading to impaired p53 activity in preadipocytes and increased proliferation, migration, and production of matrix metalloproteinase 2; treatment with MDM2 inhibitors repressed these effects. Overall, these findings indicate that MDM2 plays a crucial role in DDLPS by enabling cross-talk between tumor cells and the surrounding microenvironment and that targeting vesicular MDM2 could represent a therapeutic option for treating DDLPS.

Significance: Extracellular vesicles derived from dedifferentiated liposarcoma cells induce oncogenic properties in preadipocytes.

Introduction

Mesenchymal origin liposarcoma (LPS) is the most common human sarcoma, comprising 24% of extremity and 45% of such lesions in the retroperitoneum, respectively (1). Dedifferentiated liposarcoma (DDLPS) poses a remarkable clinical challenge due to frequent large growth before clinical detection and the lack of any new and effective therapeutics. Since the early 1970s, treatments consist of radical surgery, adjacent organ radiotherapy of undefined overall and disease-free survival impact, with the potential to damage adjacent organs, and untargeted toxic, marginal efficiency, systemic therapies. DDLPS is especially concerning given its propensity for primarily local and occasionally distant recurrence, accounting for an overall survival rate of only 10% at 10 years (2) with approximately 1,500 new diagnoses of this lesion annually in the United States alone. Moreover, almost 60% of retroperitoneal DDLPS ultimately recur as synchronous multifocal tumors, even after initial margin-negative resection; such multicentric failures are typically beyond meaningful therapeutic interventions other than palliation (3, 4). This unique pattern of multifocal locoregional failure remains a key problem in DDLPS and the main cause of death; however, the underlying molecular mechanisms driving these multifocal recurrence processes have not been extensively explored, hampering the development of DDLPS-specific therapeutics.

In addition, no validated DDLPS patient-associated molecular biomarkers have been identified to inform prognosis, facilitate early detection of DDLPS progression or recurrence, or possibly predict therapeutic resistance (5). The American Joint Committee on Cancer staging prognostic algorithms remain defined by the same pretherapeutic clinical parameters originally introduced in the 1970s. MRI or CT scanning is used for post-therapy surveillance; these modalities frequently cannot detect or resolve early recurrence versus scarring from previous resection, causing delays in subsequent treatment initiation. At the molecular level, DDLPS is characterized by *MDM2* gene amplification with expression of WT p53; this unusual pattern is observed in approximately 10% of all human cancers, approximately 20% of soft-tissue sarcomas, and in almost 100% of dedifferentiated (DDLPS) liposarcomas (6). Although the role of *MDM2* as an oncogene has focused on its inhibition of WT p53, several studies have suggested that MDM2 may also have p53-independent roles,

[1]The James Comprehensive Cancer Center, The Ohio State University, Columbus, Ohio. [2]Department of Surgery, Division of Surgical Oncology, The Ohio State University Wexner Medical Center, Columbus, Ohio. [3]Department of Cancer Biology and Genetics, Comprehensive Cancer Center, The Ohio State University, Columbus, Ohio. [4]Department of Biomedical Engineering, College of Engineering, The Ohio State University, Ohio. [5]Department of Pediatrics and Adolescent Medicine Division of Paediatric Endocrinology and Diabetes Centre for Hormonal Disorders in Children and Adolescents, Ulm University Hospital, Germany. [6]College of Public Health, Division of Biostatistics, The Ohio State University, Columbus, Ohio. [7]Department of Surgery "B," Sheba Medical Center and The Tel Aviv University, Tel Aviv, Israel.

Note: Supplementary data for this article are available at Cancer Research Online (http://cancerres.aacrjournals.org/).

Corresponding Author: Raphael E. Pollock, The Ohio State University Comprehensive Cancer Center, James Administration D920D, 460 West 10th Avenue, Columbus, OH 43210. Phone: 614-293-7521; Fax: 614-293-3132; E-mail: raphael.pollock@osumc.edu

Cancer Res 2019;79:4911–22

doi: 10.1158/0008-5472.CAN-19-0203

perhaps in sarcoma (7), and involved pathways have yet to be extensively examined (8).

Interactions between malignant and nontransformed cells can occur within the tumor microenvironment (TME); the DDLPS microenvironment contains preadipocytes (P-a), adipocytes, macrophage (9), and other cell types. Communication between tumor and TME cells is crucial in both normal and pathologic circumstances; extracellular vesicle (EV) trafficking has emerged as one such process of tumor–microenvironment cell–cell communication (10). EVs are extruded nanoparticles involved in intercellular communication from donor to recipient cells via transfer of protein, nucleic acids, and other biologically active molecules (11). Tumor cell–derived EVs can influence noncancer cells to generate premetastatic niches that facilitate tumor dissemination and growth (12). Studies demonstrate that uptake of cancer cell EV proteins and RNA molecules can induce phenotypic changes in recipient neighboring TME cells (13–17), thereby contributing to premetastatic niche formation as sites prone to foster metastasis via tumor cell colonization. Steps in premetastatic niche formation can include the acquisition of a proinflammatory phenotype by the stroma of the metastatic niche as well as extracellular matrix remodeling through matrix metalloproteinases (MMP; ref. 18). However, to date, processes potentially contributing to DDLPS premetastatic niche formation have not yet been identified.

Against that backdrop, we evaluated *MDM2* in DDLPS-derived EVs isolated from both patient serum and DDLPS cell lines. DDLPS EV bearing *MDM2* cargo induced preadipocytes to produce MMP2, a process potentially relevant to establishing the DDLPS locoregional premetastatic niche, and thereby enabling multifocal failure in this disease.

Materials and Methods

Patients and clinical samples

Blood samples of LPS patients ($n = 16$) were collected from the Ohio State University James Cancer Medical Center, written informed consent was received from participants prior to inclusion in the study, in accordance with the Helsinki Declaration whose protocols have been approved by The Ohio State University Wexner Medical Center Institutional Review Board. Patient venous blood (12 mL) was collected in Vacutainer Plus whole blood tubes with K2 EDTA (BD). Blood serum was retrieved from the whole blood samples via centrifugation at 1,900 $g \times 10$ minutes at 4°C, then aliquoted and stored at −80°C until analysis. Healthy donor blood used in the discovery and in the validation sets was purchased from ZenBio. The detailed characteristics of patient and healthy control participants are summarized in Supplementary Tables S1 and S2. Prior to any therapy, patient pathology was confirmed using surgically resected sarcomas, and graded as per standard French Federation of Cancer Centers Sarcoma Group–Fédération Nationale des Centres de Lutte contre le Cancer (FNCLCC) criteria.

RNA/DNA isolation and RT-PCR

Total RNA from cellular samples and from EVs was isolated by using a Norgen kit and following the provided instructions (Norgen BioTek). For cell line–derived EVs, RNA was isolated by using the Norgen kit as described above. Total DNA derived from tissues, cell lines, and EVs was isolated by using the Qiagen kit following the manufacturer's protocol.

The expression level of an individual gene starting from RNA preparation was determined using RNA sequence–specific probes (MDM2- Hs01066930_m1; GAPDH- Hs00266705_g1 Thermo Fisher) as per quantitative real-time RT-PCR–based detection methodology. Total RNA was reverse transcribed by using TaqMan Advanced mRNA cDNA Synthesis Kit (Thermo Fisher), according to the manufacturer's protocol. GAPDH (Hs00266705_g1, Thermo Fisher) and/or ACTB (Hs99999903_m1, Thermo Fisher) was used to normalize quantitative Real-Time PCR on RNA cellular samples. The expression level of an individual gene starting from a DNA preparation was determined using DNA sequence–specific probes (*MDM2*- Hs00540450_s1, Thermo Fisher). As for the real time of *MDM2*-DNA from cellular EVs, the same quantity of vesicles was used (calculated by nanosight), and the results were normalized on GAPDH (Hs03929097_g1, Thermo Fisher). Determination of the number of molecules of *MDM2* in the serum EVs was performed using standard curve methodology (Supplementary Fig. S1A–S1C). For the RT-PCR on the DNA EVs of the serum, the normalization was volumetrically performed. All samples were run in triplicate.

Cell culture

Human LPS cell lines Lipo246, Lipo863, and Lipo224 were established in our laboratory as previously reported (19). SW872 cells were obtained from ATCC. Cells were maintained using standard conditions and were grown in DMEM (Gibco), supplemented with 10% (vol/vol) FBS. Two sources of human P-a were used. All the experiments were performed using both cell lines, unless indicated otherwise. Human preadipocytes (XA15A1) were purchased from Lonza and maintained following the manufacturer's instructions. SGBS P-a instead (20) were cultured in DMEM/Ham's F12 (1:1) containing 33 μmol/L biotin, 17 μmol/L pantothenate, antibiotics (serum-free, basal medium), and 10% FBS. All the cell lines used in this study were acquired within the past 5 years and authenticated by STR on July 14, 2018. All cell lines were tested for *Mycoplasma*.

EV isolation and treatments

EVs were isolated according to He and colleagues (21). Serum-derived vesicles were isolated by using ExoQuick (System Biosciences), following the manufacturer's protocol. The quality and size of isolated particles were assessed through nanosight, and EV size assessment was performed with nanosight, while we verified the purity of isolated particles by Western blot (Supplementary Fig. S2A–S2C). For treatments with GW4869 (Sigma), Lipo246 cells were incubated with GW4869 5 μmol/L diluted in FBS-depleted medium for 48 hours (as in Casadei and colleagues, ref. 9), then EVs were isolated through ultracentrifugation. For all cellular treatments, P-a were seeded in a 12-well plate; after 24 hours they were treated with isolated EVs for 72 or 96 hours; SAR405838 (Sanofi-Aventis) was added at a final concentration of 0.2 μmol/L as proposed by Bill and colleagues (22).

Western blotting

For immunoblotting analysis, cells were lysed with ice-cold NP-40 Cell Lysis Buffer (Invitrogen) supplemented with protease inhibitors (Roche) for 30 minutes at 4°C. Equivalent amounts of protein were first mixed with sample buffer, then loaded on a Criterion Tris-HCl 4%–20% precast gel (Bio-Rad) and transferred to PVDF or nitrocellulose membranes. Membranes

were incubated overnight at 4°C with commercially available antibodies as indicated per experiment: anti-p53 (MA5-14516, Invitrogen) -p21 (#SC-756, Santa Cruz); -MDM2 (#MA1-113, Invitrogen); -GAPDH (#SC-48167, Santa Cruz); -β-actin (#SC-1616, Santa Cruz) -calnexin (#C7617, Sigma); -CD9 (#D8O1A, Cell Signaling Technology); -Alix (#SAB4200476, Sigma); -TSG101 (#T5701, Sigma). The proteins of interest were detected through chemiluminescence reaction. The band density of proteins was quantified using densitometric software (Odyssey, LI-COR Biosciences) or ImageJ.

MTS, migration assays, and cell cycle

Cell proliferation was performed as described previously (9). Cell migration was assessed by using transwell migration chamber (Corning). Briefly, P-a were diluted in serum-free medium and seeded in the transwell upper chamber following different conditions (EV-depleted medium, Lipo246-derived EVs, Lipo863-derived EVs, EVs with or without SAR405838, EVs derived from the serum of healthy donors or from DDLPS patients). The lower chamber was filled with medium supplemented with 10% FBS. After 72 hours, filters were washed, fixed, and stained with Coomassie Brilliant Blue (Sigma-Aldrich Corp.). Migrated cells in the lower surface of the filter were analyzed using ImageJ. For SAR405838 treatment, isolated EVs were suspended in medium (without FBS) where SAR405838 at a concentration of 0.2 μmol/L was added (22). For cell-cycle analysis, cells were harvested, washed, and fixed and then stained with 50 μg/mL propidium iodide (Sigma-Aldrich Co.) for 30 minutes. Cells were analyzed in a FACSCalibur, and data were analyzed with ModFitLT v3.1 software (Verity Software House).

Copy-number variation assay

Assessment of copy-number variation (CNV) quantified genomic *MDM2* amplification in DDLPS tissues. Isolated genomic DNA samples were measured for concentration and quality using the Cytation 3 spectrophotometer (BioTek Instruments). Samples were diluted to 5 ng/μL with nuclease-free water, and assessed using the *MDM2* copy-number probe (item# Hs06365580_cn, cat. # 4400291, Thermo Fisher Scientific) with the associated TaqMan Copy-Number Assay kit (Thermo Fisher Scientific) in the StepOnePlus Real-Time PCR System (Applied Biosystems).

Molecular number variation

We used RT-PCR to calculate the number of molecules of *MDM2* DNA in the EVs of the serum, following the methodology as per Dubois and colleagues (23). First, we performed serial dilution of *MDM2* synthetic oligo and calculated the number of molecules of *MDM2* that correspond to each different concentration. Then, an RT-PCR using *MDM2* probe (Hs03929097_g1, Thermo Fisher) was performed using these diluted synthetic oligo samples (Integrated DNA Technologies). A standard curve was then constructed in which a specific number of molecules was assigned based on the corresponding C_t value (Supplementary Fig. S1A–S1C).

Gelatin zymography

Protein content of the isolated conditioned medium (CM) samples was quantified by μBCA according to the manufacturer's protocol (Thermo Fisher Scientific). Gelatin zymography was performed as described by Deshmukh and Toth (24, 25). Briefly, 30 μg of protein collected from the CM was loaded onto precast gelatin zymography gels (10% polyacrylamide, 0.1% gelatin; Thermo Fisher Scientific). Samples were electrophoresed for 2 hours at 120 V at 4°C. Gels were then washed three times for 10 minutes in renaturing buffer containing 2.5% Triton X-100 in 50 mmol/L Tris-HCl (pH 7.5), to allow the proteinases to renature. Gels were then transferred to a developing buffer solution containing 1% Triton X-100, 1 μmol/L $ZnCl_2$, and 5 mmol/L $CaCl_2$ in 50 mmol/L Tris-HCl (pH 7.5) overnight at 37°C, under gentle agitation. After 24 hours, gels were stained with 0.5% (w/v) Coomassie Brilliant Blue (Thermo Fisher Scientific) in a solution of deionized water, methanol and acetic acid (50/40/10 v/v) for 2 hours at room temperature. Gels were destained in the same solution, but without Coomassie Blue, for 10 minutes. Images were captured using a FluorChem E gel imager (Protein Simple) using the UV transilluminator (365 nm). Band intensities were quantified using ImageJ software as described by Ren and colleagues (26) and normalized with respect to untreated condition.

DNA plasmids, virus production, and transduction

Nontargeting control vector plasmid and shRNA targeting endogenous human *MDM2* transcript were obtained from Origene. Both plasmids were packaged in Lenti-X 293T cell line (Clontech) by transfection with Lenti-X Packaging Single Shots (VSV-G; Clontech). Lipo863 cells were then transduced with lentiviral particles in the presence of polybrene 8 μg/mL (Sigma). The medium was replaced 24 hours after transduction.

Sequencing

MDM2 sequencing was analyzed by PCR amplification and subsequent DNA sequencing of exons 1, 6, 10 (using primers built on the introns before and after each exon, primers description in Supplementary Table S3). PCR products were purified with the QIAquick PCR Purification Kit (Qiagen) according to the manufacturer's specifications. DNA sequencing was performed by the Genomic Shared Resource at the Ohio State Unversity Comprehensive Cancer Center.

Statistical analysis

Differentially amplified genes and differentially expressed mRNAs between comparison groups were determined by two-sided *t* tests and fold changes using log-transformed values. Unpaired *t* test with Welch correction was applied in serum and tissue sample analysis. A one-way ANOVA with Dunnett multiple comparison test was applied to the analysis of gelatin zymography. We also calculated the area under the ROC of each ROC curve. AUC is the average sensitivity of the biomarker over the range of specificities that used as a summary statistic representing the overall performance of the biomarker. AUC of a biomarker with no predictive value would be 50%, whereas a biomarker with an AUC of 100% would indicate perfect ability to predict disease.

Results

DDLPS patient serum–derived EVs contain high levels of *MDM2* DNA

The molecular hallmarks of DDLPS are high levels of *MDM2* concomitant with WT p53, a finding observed in nearly 100% of DDLPS tumors (6). However, the content of DDLPS EVs has not yet been assessed; thus, we examined EVs isolated from DDLPS patient serum for the presence of *MDM2* DNA as compared with normal individual control serum-derived EVs ($N = 16$ DDLPS

patients and 6 healthy controls). Isolated EVs were characterized by nanosight and showed particle sizes in the characteristic 30 to 100 nm range (Supplementary Fig. S3; details regarding patient and healthy control characteristics are described in Supplementary Tables S1 and S2). The standard method to assess the DNA level of *MDM2* is by the determination of CNV (27). However, the lack of a calibrator sample (a gene of known and stable copy number) contained within the EVs meant this CNV could not be used to determine the levels of *MDM2* DNA in the DDLPS EVs. Consequently, RT-PCR incorporating a standard curve methodology was used to calculate a specific threshold cycle (C_t value) that corresponded to the number of EV *MDM2* DNA molecules (Supplementary Fig. S1) within the EVs of both DDLPS patients and healthy control groups. Our results showed that the number of *MDM2* DNA molecules present in DDLPS patients was significantly higher versus healthy counterparts ($P \leq 0.001$; Fig. 1A). Interestingly, this increase was also concordant with the *MDM2* CNV as measured in DDLPS tissues ($N = 14$) compared with normal adjacent tissues ($N = 5$; $P \leq 0.0045$; Fig. 1B; details of patients and normal controls are described in Supplementary Tables S4 and S5). EV DNA sequencing of the entire exons 1, 6, 10 of *MDM2* (using primers built on the introns before and after each exon; primer descriptions in Supplementary Table S3) showed the presence of *MDM2* DNA within the isolated serum EVs (Fig. 1C).

ROC curve analysis was conducted on the serum EVs data obtained from RT-PCR, to estimate the sensitivity and specificity of circulating EV-*MDM2* to discriminate DDLPS patients from controls (Fig. 1D). The AUC for *MDM2* was 95.8% with a 95% confidence interval from 86.9% to 100%, indicating robust separation between the DDLPS and healthy controls.

DDLPS cells constitutively shed EVs enriched in *MDM2* DNA

Previously, we showed that DDLPS cell lines release EVs (9). To verify the DDLPS tumor origin of *MDM2* EVs isolated from the serum of DDLPS patients, we collected CM from different DDLPS cell lines, isolated the EVs by ultracentrifugation, and assessed *MDM2* content. EV DNA sequencing of the entire exons 1, 6, 10 of *MDM2* (using primers built on the introns before and after each exon; primer descriptions in Supplementary Table S3) demonstrated the presence of *MDM2* DNA within isolated EVs (Fig. 2A). EV size assessment was performed with nanosight, demonstrating particle sizes in the characteristic 30- to 100-nm range (Supplementary Fig. S2A), whereas we verified the purity of isolated particles through the detection of typical EV proteins by Western blot (Supplementary Fig. S2B and S2C). The low expression levels of cell normalizers such as RNU48, RNU6, and RNU44 within isolated vesicles confirmed the absence of cell contamination in the EV preparations (Supplementary Table S6; ref. 9). When measured using RT-PCR, the level of *MDM2* DNA EVs secreted by DDLPS cell lines (Lipo863, Lipo246, and Lipo224) demonstrated consistent and significant upregulation compared with the level of *MDM2* DNA in P-a-derived EVs and LPS SW872-derived EVs ($P \leq 0.01$; Fig. 2B). Furthermore, the level of *MDM2* DNA in EVs was proportional to the level of *MDM2* in the cells of EV origin ($P \leq 0.0001$; Fig. 2C). The quantity of *MDM2* DNA was calculated by RT-PCR, using the same amount of EVs for each cell line (calculated by nanosight) and normalized for GAPDH DNA. Taken together, these data indicate that DDLPS cells release EVs with high levels of *MDM2* DNA that reflect the levels of MDM2 in the DDLPS cells. We then wanted to make sure that the increased level of *MDM2* considered its DNA form, rather than mRNA or protein. So we measure the quantity of mRNA and proteins also in the isolated DDLPS EVs. Although we were able to detect a high level of *MDM2* in DDLPS EVs at the DNA level, the amount of MDM2 mRNA was much lower and the amount of MDM2 protein was undetectable.

DDLPS cell EV cargo *MDM2* DNA is transferred to normal P-a

Because DDLPS predominantly arise in fat-bearing areas of the retroperitoneum in which the TME is enriched for P-a, we wanted to determine whether *MDM2* DNA was transferred from DDLPS EVs to P-a. P-a were incubated with Lipo246-derived EVs for 72 hours. When we assessed the expression level of MDM2 mRNA within the recipient P-a cells, we observed that it was significantly increased compared with P-a incubated with EV-depleted medium ($P \leq 0.001$; Fig. 3A). To further demonstrate the transfer of *MDM2* DNA from DDLPS to P-a, we treated the latter with increased amount of Lipo-246–derived EVs and determined the MDM2 mRNA expression level in the recipient cells. As shown in Fig. 3B, the level of MDM2 in recipient P-a increased in proportion to the amount of Lipo246 EVs added. Finally, to verify whether the *MDM2* DNA transfer led to an increased production of MDM2 protein within recipient P-a, we performed a Western blot analysis of P-a lysates derived from cells incubated for 72 and 96 hours with Lipo-246-derived EVs (Fig. 3C; Supplementary Fig. S4). These studies showed that the level of MDM2 protein increased in incubated P-a in a time-dependent manner, reaching a 3-fold incremental change compared with untreated P-a (P-a treated with EV-depleted medium). Taken together, these data indicate that *MDM2* DNA was transferred from DDLPS EVs to P-a as a biologically active molecule capable of being translated into MDM2 protein within the P-a cells.

Transfer of EV *MDM2* DNA leads to downregulated P-a p53 activity

We next examined whether *MDM2* DNA, upon translation into MDM2 protein in recipient P-a, could downregulate P-a p53 activity (Fig. 3D). Using Western blot, we determined the amount of p53 and p21 protein in P-a exposed to DDLPS EVs for 96 hours under different conditions. As shown in Fig. 3D, incubation of P-a with Lipo246 EVs for 96 hours led to decreased p53 and p21 protein levels (lane 3) compared with treatment with EV-depleted medium (lane 1). Next, we considered whether MDM2 was at least partially responsible for these changes. The selective MDM2 inhibitor SAR405838 blocks p53:MDM2 interaction at the protein level by occupying the MDM2 p53 binding site (28), causing an increase in both P-a p53 and p21 expression (lane 2). To confirm the mechanism of action of the MDM2 inhibitor (SAR405838), a Western blot showing a concomitant increase in MDM2 protein expression after treatment with the MDM2 inhibitor is also provided (Supplementary Fig. S5). When P-a were treated with Lipo246 EVs and SAR405838 for 96 hours, the EV inhibitory effect on p53 and p21 was abrogated (lane 4) compared with P-a treated with Lipo246 EVs (in lane 3), suggesting that uptake of *MDM2* DNA by P-a inhibited p53 and p21 expression. P-a treatment with EVs isolated from Lipo863, a DDLPS cell line whose *MDM2* levels are much lower than these of Lipo246 (see Fig. 2B and C), produced p53 and p21 results more closely resembling P-a treated with Lipo246 EV+ SAR405838 (lane 5). Interestingly, when P-a were incubated with EVs derived from Lipo863 transduced with lentiviral particles for the overexpression of MDM2 (see Materials and Methods;

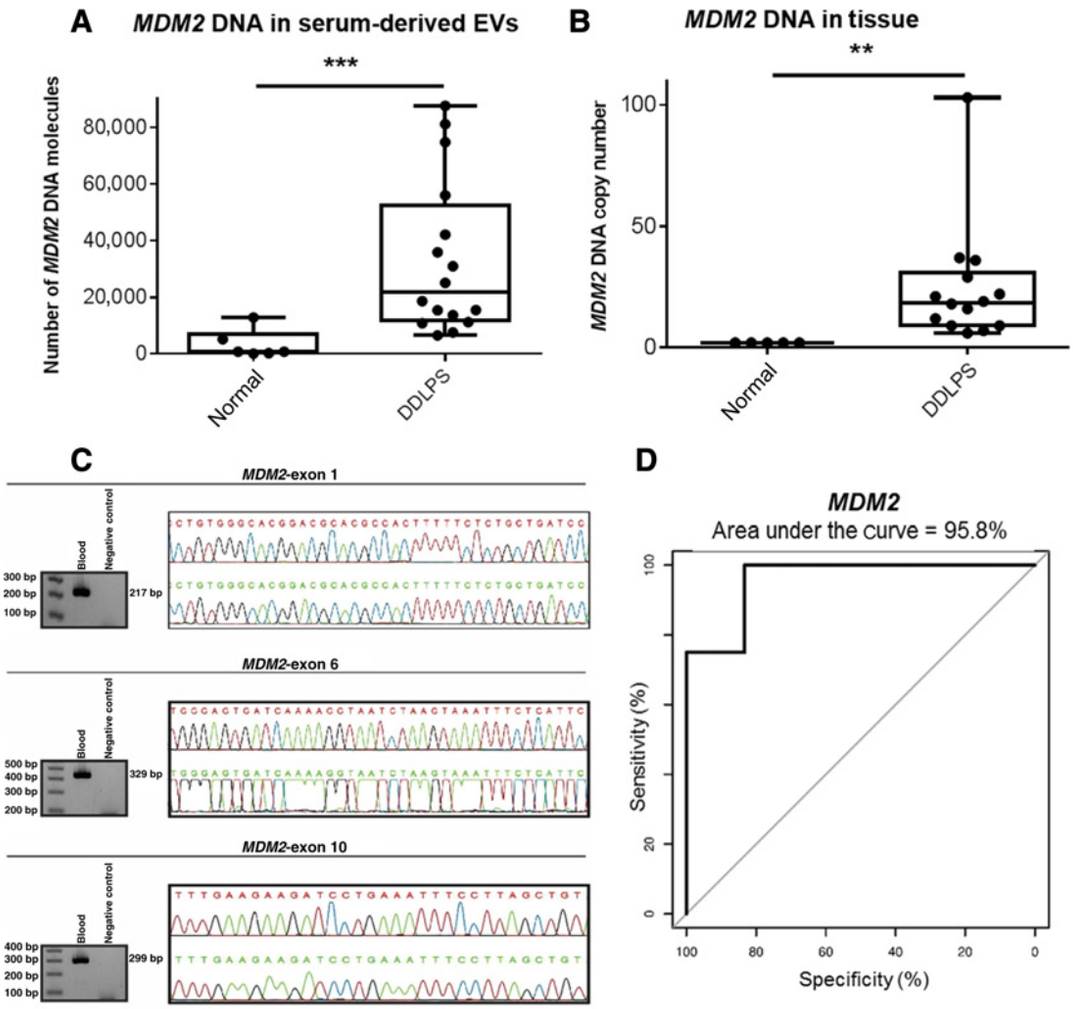

Figure 1.

DDLPS patient serum–derived EVs contain high level of *MDM2* DNA. **A,** RT-PCR representing the number of molecules of *MDM2* in DDLPS patient serum EVs ($n = 16$) compared with normal healthy controls ($n = 6$; $P \leq 0.001$). **B,** *MDM2* CNV measured in DDLPS tissues ($n = 14$) compared with normal adjacent tissues ($n = 5$; $P \leq 0.0045$). **C,** EVs derived from DDLPS patient serum contain *MDM2* by DNA sequencing on the entire exons 1, 6, and 10 of *MDM2*. **D,** ROC curve analysis to estimate the sensitivity and specificity for circulating EV-*MDM2* in discriminate DDLPS patients from controls. Results are presented as average ± SEM. Statistical analyses were performed using an unpaired *t* test with Welch correction. **, $0.001 \leq P \leq 0.01$; ***, $P \leq 0.001$.

Supplementary Fig. S6), the level of p53 and p21 decreased again resembling P-a treated with Lipo246 EVs (lane 6). These data suggest that DDLPS EVs induce downregulated p53 activity, which was due to *MDM2* DNA transfer from DDLPS to recipient P-a per se.

EV-origin transferred *MDM2* DNA confers oncogenic features in normal recipient P-a

Next, we asked whether the transfer of *MDM2* DNA within DDLPS-derived EVs conferred DDLPS cell pro-oncogenic features to normal P-a cells. P-a were incubated for 72 hours with EVs isolated from Lipo246 cells; when proliferation and migration was assessed, P-a exhibited enhanced proliferation and migration ($P \leq 0.0001$), compared with cells incubated with EV-depleted medium or media alone (Fig. 4A and B). When P-a were incubated for 72 hours with EVs in the presence of the MDM2 inhibitor SAR405838, the rate of proliferation and migration of recipient cells was significantly impaired compared with EV treatment only, suggesting that this characteristic was dependent on *MDM2* DNA transfer. Furthermore, P-a treated with Lipo863 EVs (whose *MDM2* levels are lower compared with Lipo246; Fig. 2B and C) displayed impaired proliferation ($P \leq 0.03$) and migration ($P \leq 0.001$) compared with Lipo246-EV treatment. To confirm these results, we treated P-a with EVs isolated from pooled DDLPS patient serum ($N = 8$) and compared proliferation and migration versus P-a treated with EVs isolated from pooled healthy donor serum and P-a treated with media alone ($N = 3$; patient and healthy donor clinical information are presented in Supplementary Tables S8 and S9; RT-PCR was used to assess the number of molecules of *MDM2* in the EVs of both patient and normal pooled serum; Supplementary Fig. S7). As depicted in Fig. 4C and D, incubation for 72 hours with patient serum-derived EVs significantly increased P-a proliferation and migration compared with cells incubated with EVs derived from normal

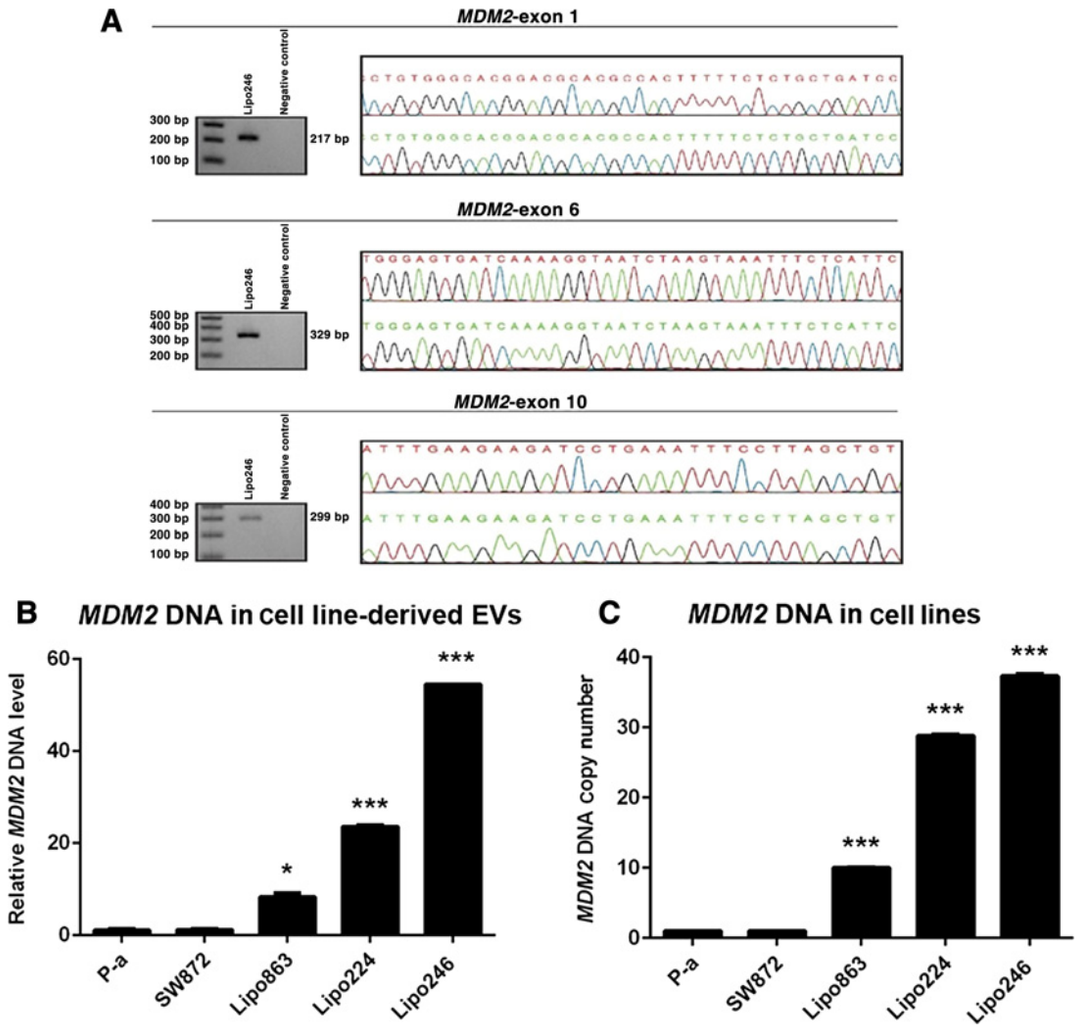

Figure 2.

DDLPS cells constitutively release EVs carrying *MDM2* DNA. **A,** EVs derived from Lipo246 contain *MDM2* by DNA sequencing on the entire exons 1, 6, and 10 of *MDM2*. **B,** Level of *MDM2* (calculated by RT-PCR) in DDLPS-secreted vesicles (Lipo863, Lipo246, and Lipo224) is consistently and significantly upregulated compared with the level of *MDM2* DNA in P-a–secreted EVs ($P \leq 0.01$). The level of *MDM2* in EVs is proportional to the level of *MDM2* in the originating cells. **C,** Level of *MDM2* in different LPS cell lines calculated by CNV ($P \leq 0.0001$). Results are presented as average ± SD. Statistical analyses were performed using *t* test. *, $0.01 < P < 0.05$; ***, $P \leq 0.001$.

controls and media alone ($P \leq 0.005$ and $P \leq 0.0001$, respectively). To mechanistically explain the increase in cellular proliferation following *MDM2* transport to the P-a, cell-cycle analysis by FACS was performed. As depicted in Fig. 4E; Supplementary Table S7, incubation of P-a with Lipo246 EVs induces a 3-fold increase in the S phase compared with normal medium or depleted medium P-a treatment ($P \leq 0.01$). Taken together, our data suggest that DDLPS EV *MDM2* can contribute to oncogenic features such as enhanced P-a proliferation and migration.

Transfer of EV-origin *MDM2* DNA promotes production of MMP2 by P-a

EVs contribute to facilitate premetastatic niche establishment and maintenance (29). The nearly 60% rate of DDLPS multifocal locoregional recurrence is remarkably high among all solid tumors. However, the reason for this extremely high rate remains unknown. Several factors, including MMPs, have been identified as contributing to premetastatic niche formation. Therefore, we wanted to further explore the consequences of DDLPS EV interaction with P-a to see if other processes relevant to multifocal DDLPS locoregional recurrence might also be induced.

To verify whether EVs stimulated P-a to release active MMPs, we incubated P-a with Lipo246-EVs and Lipo224-EVs for 96 hours and then performed gelatin zymography analysis with the resultant CM. We found that active MMP2 (62 kDa) was significantly overproduced in the CM derived from EV-treated P-a versus P-a treated with EV-depleted medium (Fig. 5). To verify that EV-derived *MDM2* was the driver of the enhanced MMP2 activity, we also treated P-a with DDLPS-derived EVs (Lipo246 EVs) in the presence of the MDM2 inhibitor SAR405838 (0.2 μmol/L for 72 hours); this treatment strongly impaired the release of active MMP2 (Fig. 5). When P-a were treated with

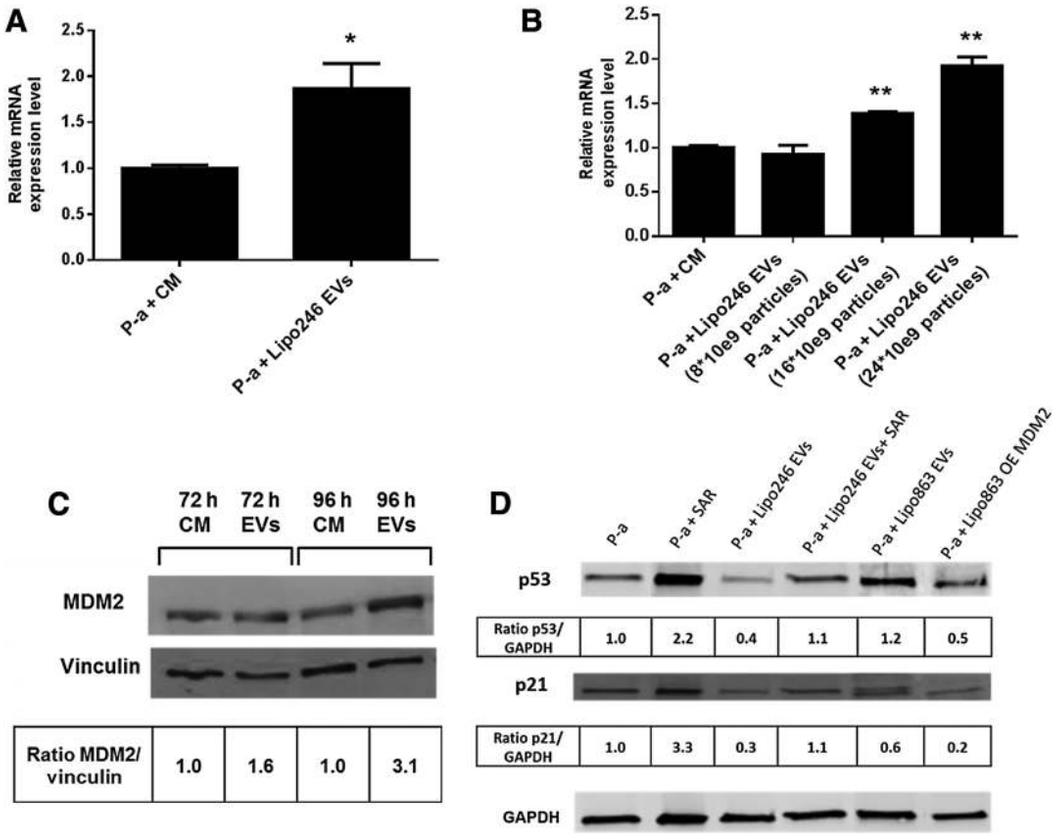

Figure 3.

DDLPS cell EV cargo *MDM2* DNA is transferred to recipient P-a and affects intracellular pathway downstream of MDM2. **A,** Level of MDM2 (measured by RT-PCR) in recipient P-a increases at mRNA level when P-a are treated with Lipo246 EVs for 72 hours ($P \leq 0.04$). **B,** Recipient P-a treated with Lipo246 EVs for 72 hours show an increased level of MDM2-mRNA in a dose–response manner ($P \leq 0.002$). **C,** When P-a are treated with Lipo246 EVs, the protein level of MDM2 increases 3-fold after 96 hours. Results are presented as average ± SD. Statistical analyses were performed using *t* test. *, $0.01 < P < 0.05$; **, $0.001 \leq P \leq 0.01$. **D,** When P-a are treated with Lipo246-EVs (for 96 hours), they show a decreased level of p53 and p21 compared with untreated P-a (lane 3). When P-a are treated with Lipo246-EVs together with MDM2 inhibitor (SAR405838, 0.2 μmol/L), the inhibitory effect of EVs on p53 and p21 is rescued (lane 4). Treatment of P-a with EVs isolated from Lipo863 (whose *MDM2* levels are lower compared with Lipo246) produces results analogous to the treatment of P-a with SAR405838 (lane 5). When P-a are treated with EVs isolated from Lipo863, where MDM2 is overexpressed, the level of p53 and p21 decreases again (lane 6).

EVs isolated from Lipo246 previously treated with GW4869 (a drug that blocks EV secretion; ref. 30), the release of active MMP2 was impaired. Moreover, when P-a were treated with Lipo863 EVs (whose *MDM2* levels are lower compared with Lipo246; Fig. 2B and C), active MMP2 release was strongly impaired (Fig. 5A and B). In contrast, when P-a were treated with EVs isolated from Lipo863 transduced with lentiviral particles for the overexpression of MDM2 (see Materials and Methods), active MMP2 release was strongly increased (Fig. 5A and B). Of note, the appearance of an active pro-MMP2 in the zymograms is an artifact of the electrophoretic process per se; this species would be inactive under physiologic conditions. SDS-containing zymography buffer results in denaturation of the proteins during electrophoresis. Upon removal of SDS during the zymogram development phase, the proteins renature, partially refold and become active. As such, both the higher molecular weight pro-MMP2 (72 kDa) band and the active MMP2 (62 kDa) band can be visualized for some preparations in the zymograms depicted in Fig. 5A. Finally, it is also pertinent to note that gelatin zymography is a semiquantitative process and is constrained in its detection limits for MMP2; it is possible that other preparations could generate MMP2 activity that is below the threshold of detectability using gelatin zymography.

Taken together, our findings support the premise that P-a uptake of DDLPS EV-derived *MDM2* DNA increases MMP2 secretion in recipient P-a cells, a potential factor contributing to the establishment of multifocal locoregional premetastatic niches, especially given the widespread P-a presence throughout retroperitoneal and abdominal fat-bearing areas of DDLPS patients.

EV-exposed P-a media promote DDLPS proliferation

After establishing that DDLPS EVs promote an oncogenic phenotype in P-a, we wanted to verify also whether the induction of this oncogenic phenotype, together with MMP2 activation, had any implication regarding disease progression. Therefore, proliferation assays were performed using DDLPS cells treated with media collected from P-a previously exposed to EVs. As shown in Fig. 6, when Lipo246 and Lipo224 cells were treated with Lipo246-EV and Lipo224-EV exposed P-a medias for 48 hours, respectively, they showed increased proliferation ($P \leq 0.001$)

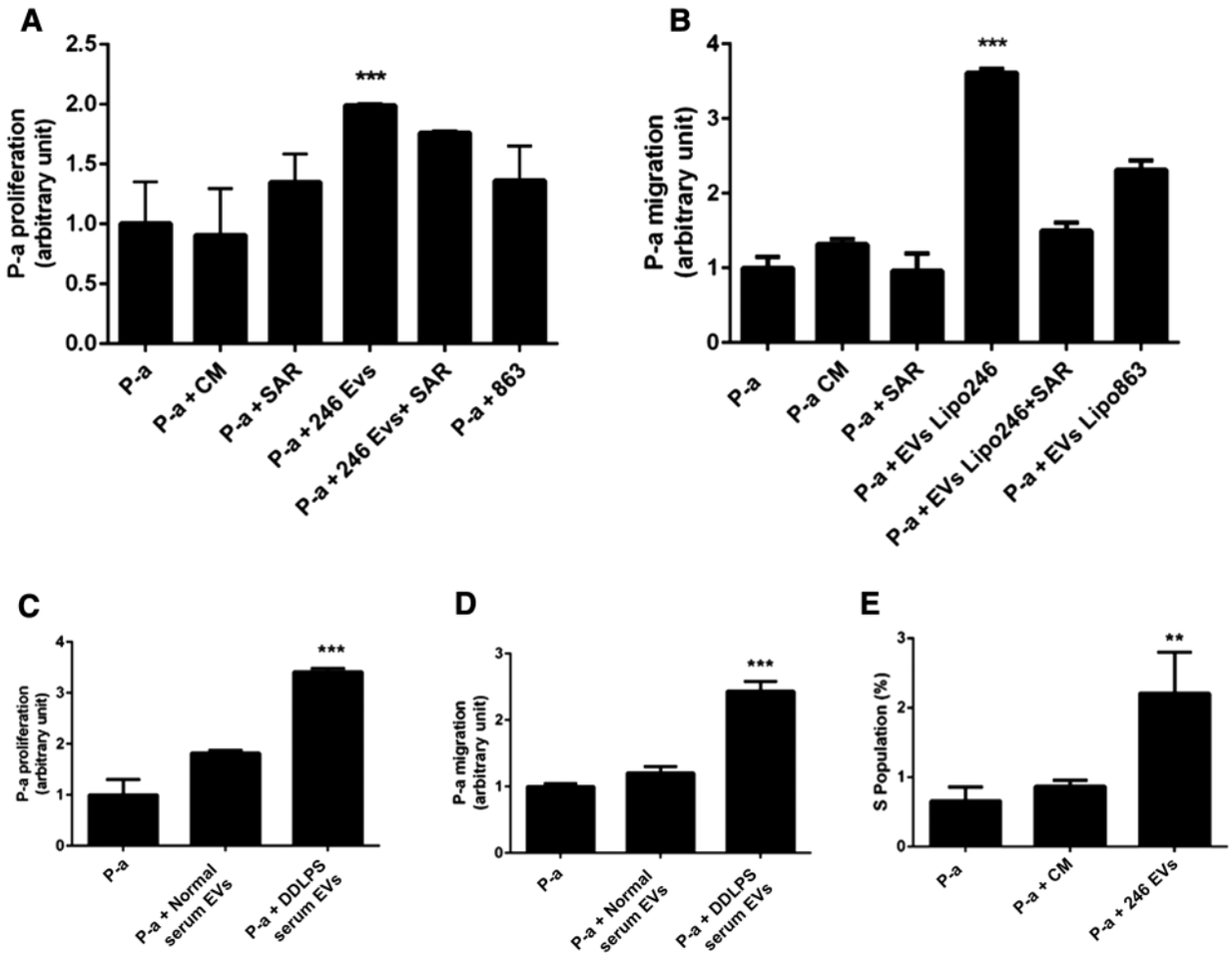

Figure 4.

MDM2 cargo confers oncogenic features in normal recipient P-a. **A,** EVs increase P-a proliferation. When *P*-a are treated with Lipo246 EVs for 72 hours, they show increased proliferation ($P \leq 0.0001$) compared with P-a treated with EV-depleted medium (Pa + CM) and media alone (P-a). **B,** Lipo246 EVs promote migration in recipient P-a. When P-a are treated with Lipo246-EVs, they show an increased migration compared with P-a treated with EV-depleted medium (Pa + CM) and media alone (P-a). Furthermore, P-a treated with Lipo246-EVs together with an MDM2 inhibitor (SAR405838, 0.2 μmol/L) show a decreased migration compared with P-a treated with Lipo246-EVs without drug ($P \leq 0.05$). P-a treated with drug alone do not have a significant change in migration compared with P-a treated with EV-depleted medium. P-a treated with Lipo863 EVs (whose *MDM2* levels are lower compared with Lipo246) have decreased migration compared with P-a treated with Lipo246 EVs. P-a treated with EVs isolated from a pool of serum derived from DDLPS patients ($N = 8$) have increased proliferation ($P \leq 0.0001$; **C**) and migration ($P \leq 0.005$; **D**) compared with P-a treated with EVs isolated from a pool of normal serum ($N = 3$) and compared with P-a treated with media alone. **E,** Cell-cycle analysis of P-a by FACS. Treatment with Lipo246 EVs induces increase in S phase compared with normal medium or EV-depleted medium. Results are presented as average ± SD. Statistical analyses were performed using *t* test. **, $0.001 \leq P \leq 0.01$; ***, $P \leq 0.001$.

compared with untreated Lipo246 and Lipo224 as well as when compared with DDLPS cells incubated with P-a derived CM originating from P-a treated with Lipo246 or Lipo224 EV-depleted media. On the contrary, incubation of Lipo863 with Lipo863-EV exposed P-a media did not change Lipo863 growth, suggesting that the observed increased growth is possibly due to changes induced by DDLPS EV-derived from cell lines bearing high levels of *MDM2*.

Discussion

The vast majority of DDLPS contain WT p53 whose tumor suppressor function is impaired by the marked overproduction of MDM2 at both the DNA and protein levels. Highlighting this specific oncobiology, FISH assessment of *MDM2* is currently the definitive diagnostic methodology for DDLPS. Almost 60% of retroperitoneal DDLPS ultimately recur as synchronous multifocal tumors, even after initial margin-negative resection; this deleterious locoregional metastatic outgrowth, whose mechanism is unknown, remains the major cause of DDLPS lethality (3, 4).

Here we examined the oncobiologic significance of DDLPS EV-derived *MDM2* in the circulation, demonstrating that DDLPS patients produce significantly increased amounts of *MDM2* DNA in their EVs compared with normal controls. To date, no validated DDLPS patient-associated molecular

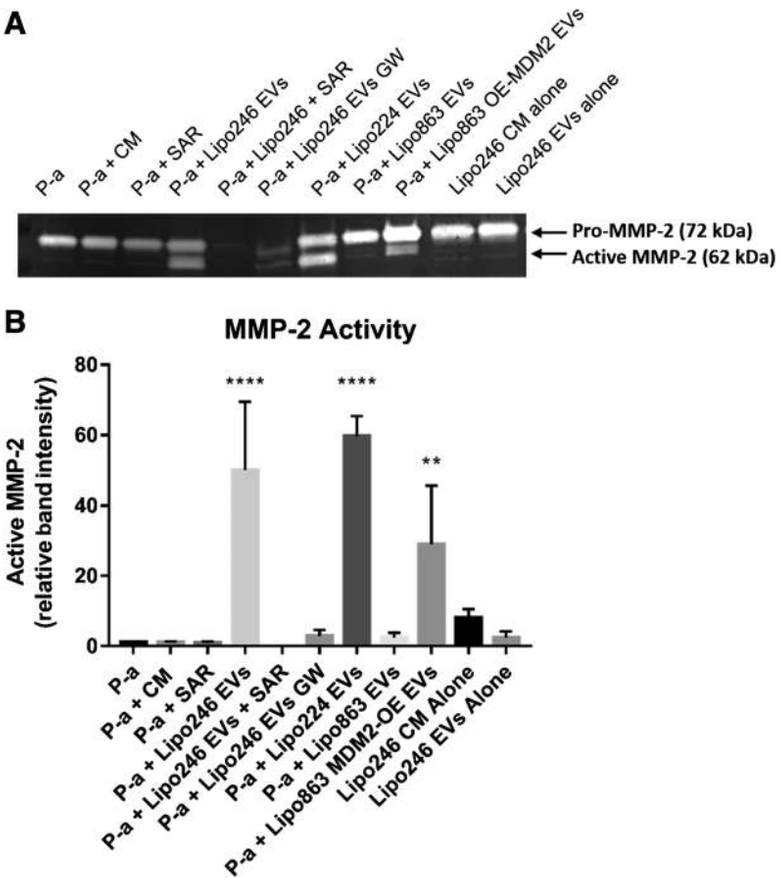

Figure 5.

Uptake of *MDM2*-EVs by P-a induces MMP-2 activation. **A,** Zymography showing increase of active MMP-2 released by P-a after EV incubation for 96 hours. MMP-2 activity (active MMP-2, 62 kDa) was significantly enhanced in the medium of Lipo246-EVs and Lipo224-treated P-a compared with P-a treated with EV-depleted medium (P-a + CM) and P-a alone (P-a). The treatment with the MDM2 inhibitor SAR405838 (0.2 μmol/L) impaired the release of active MMP-2. When P-a are treated with Lipo246-EVs after incubation of DDLPS cells with GW4869 (a drug that blocks EVs generation), the active MMP-2 released decreases as well as when P-a are treated with EVs isolated from Lipo863 (whose *MDM2* level are lower compared with Lipo246). The level of active MMP-2 is rescued when P-a are treated with Lipo863 EVs where MDM2 is overexpressed. Representative images, experiments performed at least three times. In **B**, results are presented as average ± SD. Statistical analyses were performed using a one-way ANOVA with Dunnett multiple comparisons test. **, $P \leq 0.01$; ****, $P \leq 0.0001$.

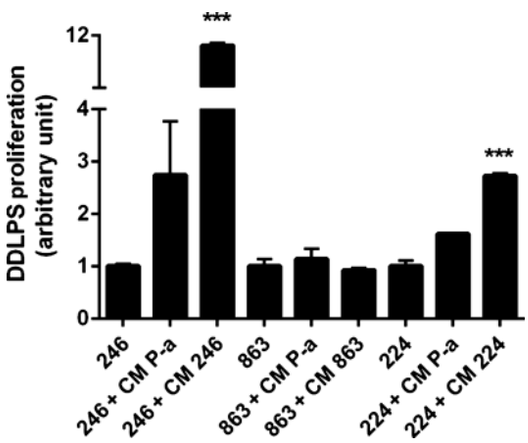

Figure 6.

EV-exposed P-a's media reciprocally promote DDLPS proliferation. When Lipo246 and Lipo224 are treated with EV-exposed P-a's media for 48 hours, they show increased proliferation compared with Lipo246 and Lipo224 treated with normal media, but also compared with each cell line treated with P-a's exposed media (CM). On the contrary, incubation of Lipo863 with Lipo863-EV–exposed P-a's media has no effect on Lipo863 growth. Results are presented as average ± SD. Statistical analyses were performed using *t* test. ***, $P \leq 0.001$.

biomarkers have been identified; consequently, this discovery suggests that circulating EV *MDM2* may serve as a biomarker, perhaps informing prognosis and facilitating early detection of DDLPS progression or recurrence, or possibly even predicting therapeutic resistance.

We also demonstrated that DDLPS EV cargo *MDM2* could be transferred to recipient P-a (one of the most prominent cells in the DDLPS microenvironment); P-a treated with DDLPS EV-origin *MDM2* expressed both increased MDM2 mRNA as well as increased amounts of MDM2 protein in a dose-dependent manner. This discovery is consistent with other studies showing that tumor-secreted EVs, along with their cargos, can be internalized by other cell types in the primary tumor microenvironment as well as in recipient premetastatic niche cells where they can exert profound effects (31–33). However, to the best of our knowledge, it has not been previously shown that *MDM2* can be released from tumor-derived EVs with subsequent transfer into cells that populate the tumor microenvironment or other recipient normal cells. This study is also one of the first to demonstrate that P-a can serve as potential recipients of EV cargo, and the effect of tumor-secreted EVs on P-a has also apparently not been reported to date. Because *MDM2* is amplified in more than 40 different types of malignancies, including sarcomas, other solid tumors, and leukemias (34), our findings may be relevant to several different malignant diseases. Likewise, other diseases in which

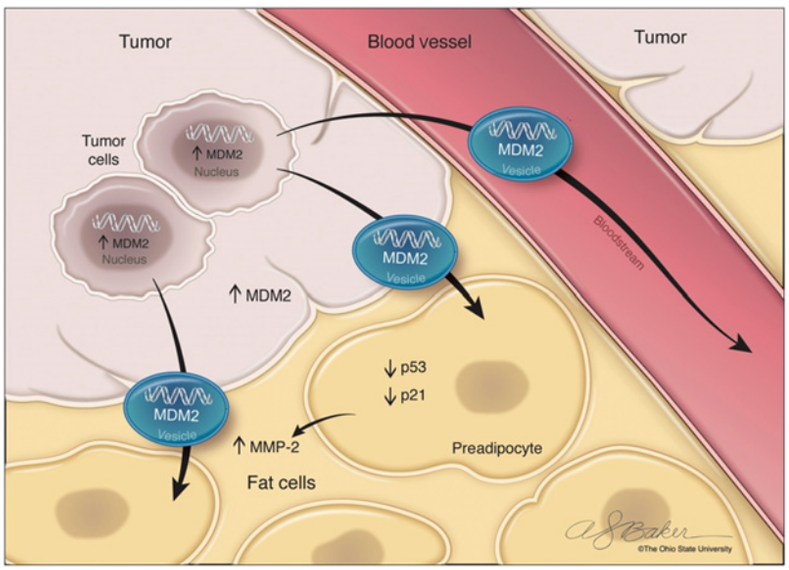

Figure 7.
Effects of EV-origin *MDM2* DNA transfer in recipient P-a. Our study establishes the presence of high level of *MDM2* DNA in DDLPS EVs derived from both DDLPS cell lines and patient serum samples. We also show that DDLPS EV *MDM2* cargo can be transferred to recipient P-a in the DDLPS TME. This DDLPS EV-origin *MDM2* leads to downregulated P-a p53 activity conferring oncogenic feature in normal recipient cells. Importantly, *MDM2* cargo promotes the release of active MMP-2 in normal recipient P-a, thereby possibly contributing to subsequent locoregional multifocal DDLPS dissemination.

TME P-a are prominent (e.g., breast cancer) could possibly have comparable clinically relevant oncobiologies.

After establishing that EVs isolated from DDLPS patient serum and cell lines both contain increased level of *MDM2* DNA levels, which can be uptaken by P-a, we showed that EV *MDM2* cargo induced MMP2 activity in recipient P-a, a previously not described relationship potentially relevant to premetastatic niche formation. MMP2 (together with MMP9) is particularly effective in degrading type IV collagen (35, 36) the major structural component of basement membranes, thus facilitating tumor invasion and metastasis. MMP2 has also been studied for its contribution to angiogenesis (37). Importantly, MMP2 has been implicated in key processes of premetastatic niche development via break down of collagen into peptides that can act as chemoattractant for circulating tumor cells (38). The role of MMP2 has also been suggested in other disseminating diseases (39–44). In the context of liposarcoma, MMP2 and MMP9 expression has been correlated with cell invasiveness (45), metastasis ($P = 0.008$ and $P = 0.005$, respectively), and grade ($P = 0.001$ and $P = 0.04$ respectively; ref. 46). Among MMP2 and MMP9, we focused on MMP2 because our results with MMP9 were inconsistent and did not achieve significance due to difficulties in MMP9 detection.

MMP2 has been shown to be enhanced by MDM2 in the context of breast cancer (47); not yet in sarcoma, where MDM2 is the key driver, the correlation between MDM2 and MMP2 has never been shown. Moreover, Bradbury and colleagues (29) describe the regulation between MDM2 and MMP2 to occur within breast cancer cells, whereas we demonstrate that *MDM2*, as a EV cargo secreted from DDLPS cells, is able to induce MMP2 production in normal P-a, a major TME component.

Our results, summarized in Fig. 7, demonstrate that DDLPS EV-origin *MDM2* induces P-a production of active MMP2, an initial demonstration of a possible regulatory relationship between tumor-derived EV *MDM2* and MMPs in normal TME component cells. We are performing studies focusing on the underlying mechanism of these *MDM2*–MMP2 interactions, hopefully leading to improved awareness of the genetic controls underlying this process.

In conclusion, we have established the presence of *MDM2* in DDLPS EVs derived from both DDLPS cell lines and also DDLPS patient serum samples. We showed that DDLPS EV *MDM2* cargo can be transferred to recipient P-a cells, leading to downregulated P-a p53 activity. Importantly, *MDM2* cargo promotes release of active MMP2 in normal recipient P-a, thereby possibly contributing to a locoregional milieu favoring multifocal DDLPS dissemination.

Disclosure of Potential Conflicts of Interest

No potential conflicts of interest were disclosed.

Authors' Contributions

Conception and design: L. Casadei, J.L. Leight, D. Lev, C.M. Croce, R.E. Pollock
Development of methodology: L. Casadei, F. Calore, P. Fadda, M. Wabitsch, D. Lev, R.E. Pollock
Acquisition of data (provided animals, acquired and managed patients, provided facilities, etc.): L. Casadei, F. Calore, D.A. Braggio, A. Zewdu, A.A. Deshmukh, P. Fadda, V.P. Grignol, R.E. Pollock
Analysis and interpretation of data (e.g., statistical analysis, biostatistics, computational analysis): L. Casadei, F. Calore, D.A. Braggio, A. Zewdu, A.A. Deshmukh, C. Song, J.L. Leight, R.E. Pollock
Writing, review, and/or revision of the manuscript: L. Casadei, F. Calore, A.A. Deshmukh, P. Fadda, M. Wabitsch, J.L. Leight, C.M. Croce, R.E. Pollock
Administrative, technical, or material support (i.e., reporting or organizing data, constructing databases): A. Zewdu, G. Lopez, C.M. Croce, R.E. Pollock
Study supervision: J.L. Leight, C.M. Croce, R.E. Pollock

Acknowledgments

Research funding in honor of Bettie Thomas Coley, a 16-year liposarcoma patient, was provided by her family: Robert Lightfoot Coley, James Lightfoot Coley, and Kathleen Coley Dinerman. We thank Michele Guescini for technical assistance. We thank Alexander Ridenour and Alex Cornwell from The Ohio State University Analytical Cytometry Shared Resources for providing support with nanosight analysis. qRT-PCR and CNV analysis were performed at The Ohio State University GSR. All the Shared Resources at The Ohio State University that contributed to this paper were supported by the Cancer Center Support Grant P30CA016058. This work was supported in part by the NCI of the

NIH (U54CA168512 to R.E. Pollock), in part by the NCI of the NIH (NIH R35CA197706 to C.M. Croce). J.L. Leight was supported by the Ohio State University CCC start-up fund 46050 502085.

The costs of publication of this article were defrayed in part by the payment of page charges. This article must therefore be hereby marked *advertisement* in accordance with 18 U.S.C. Section 1734 solely to indicate this fact.

Received January 17, 2019; revised June 14, 2019; accepted August 2, 2019; published first August 6, 2019.

References

1. Bill KL, Casadei L, Prudner BC, Iwenofu H, Strohecker AM, Pollock RE. Liposarcoma: molecular targets and therapeutic implications. Cell Mol Life Sci 2016;73(19):3711–8.r
2. Anaya DA, Lahat G, Wang X, Xiao L, Tuvin D, Pisters PW, et al. Establishing prognosis in retroperitoneal sarcoma: a new histology-based paradigm. Ann Surg Oncol 2009;16:667–75.
3. Anaya DA, Lahat G, Liu J, Xing Y, Cormier JN, Pisters PW, et al. Multifocality in retroperitoneal sarcoma: a prognostic factor critical to surgical decision-making. Ann Surg 2009;249:137–42.
4. Tseng WW, Madewell JE, Wei W, Somaiah N, Lazar AJ, Ghadimi MP, et al. Locoregional disease patterns in well-differentiated and dedifferentiated retroperitoneal liposarcoma: implications for the extent of resection? Ann Surg Oncol 2014;21:2136–43.
5. Wu JW, Preuss C, Wang SP, Yang H, Ji B, Carter GW, et al. Epistatic interaction between the lipase-encoding genes Pnpla2 and Lipe causes liposarcoma in mice. PLos Genet 2017;13:e1006716.
6. Guan Z, Yu X, Wang H, Wang H, Zhang J, Li G, et al. Advances in the targeted therapy of liposarcoma. OncoTargets Ther 2015;8:125–36.
7. Bohlman S, Manfredi JJ.p53-independent effects of Mdm2. Subcell Biochem 2014;85:235–46.
8. Marine JC, Lozano G. Mdm2-mediated ubiquitylation: p53 and beyond. Cell Death Differ 2010;17:93–102.
9. Casadei L, Calore F, Creighton CJ, Guescini M, Batte K, Iwenofu OH, et al. Exosome-derived miR-25–3p and miR-92a-3p stimulate liposarcoma progression. Cancer Res 2017;77:3846–56.
10. Maia J, Caja S, Strano Moraes MC, Couto N, Costa-Silva B. Exosome-based cell-cell communication in the tumor microenvironment. Front Cell Develop Biol 2018;6:18.
11. Cocucci E, Racchetti G, Meldolesi J. Shedding microvesicles: artefacts no more. Trends Cell Biol 2009;19:43–51.
12. Whiteside TL.Tumor-derived exosomes and their role in cancer progression. Adv Clin Chem 2016;74:103–41.
13. Al-Nedawi K, Meehan B, Kerbel RS, Allison AC, Rak J. Endothelial expression of autocrine VEGF upon the uptake of tumor-derived microvesicles containing oncogenic EGFR. PNAS 2009;106:3794–9.
14. Antonyak MA, Li B, Boroughs LK, Johnson JL, Druso JE, Bryant KL, et al. Cancer cell-derived microvesicles induce transformation by transferring tissue transglutaminase and fibronectin to recipient cells. PNAS 2011;108:4852–7.
15. Li X, Wang S, Zhu R, Li H, Han Q, Zhao RC. Lung tumor exosomes induce a pro-inflammatory phenotype in mesenchymal stem cells via NFkappaB-TLR signaling pathway. J Hematol Oncol 2016;9:42.
16. Lindoso RS, Collino F, Camussi G. Extracellular vesicles derived from renal cancer stem cells induce a pro-tumorigenic phenotype in mesenchymal stromal cells. Oncotarget 2015;6:7959–69.
17. Paggetti J, Haderk F, Seiffert M, Janji B, Distler U, Ammerlaan W, et al. Exosomes released by chronic lymphocytic leukemia cells induce the transition of stromal cells into cancer-associated fibroblasts. Blood 2015;126:1106–17.
18. Alaseem A, Alhazzani K, Dondapati P, Alobid S, Bishayee A, Rathinavelu A. Matrix metalloproteinases: a challenging paradigm of cancer management. Semin Cancer Biol 2019;56:100–115.
19. Peng T, Zhang P, Liu J, Nguyen T, Bolshakov S, Belousov R, et al. An experimental model for the study of well-differentiated and dedifferentiated liposarcoma; deregulation of targetable tyrosine kinase receptors. Lab Invest 2011;91:392–403.
20. Wabitsch M, Brenner RE, Melzner I, Braun M, Moller P, Heinze E, et al. Characterization of a human preadipocyte cell strain with high capacity for adipose differentiation. Int J Obesity Related Metab Disord 2001;25:8–15.
21. He WA, Calore F, Londhe P, Canella A, Guttridge DC, Croce CM. Microvesicles containing miRNAs promote muscle cell death in cancer cachexia via TLR7. PNAS 2014;111:4525–9.
22. Bill KL, Garnett J, Meaux I, Ma X, Creighton CJ, Bolshakov S, et al. SAR405838: a novel and potent inhibitor of the MDM2:p53 axis for the treatment of dedifferentiated liposarcoma. Clin Cancer Res 2016;22:1150–60.
23. Dubois NC, Craft AM, Sharma P, Elliott DA, Stanley EG, Elefanty AG, et al. SIRPA is a specific cell-surface marker for isolating cardiomyocytes derived from human pluripotent stem cells. Nat Biotechnol 2011;29:1011–8.
24. Deshmukh AA, Weist JL, Leight JL. Detection of proteolytic activity by covalent tethering of fluorogenic substrates in zymogram gels. BioTechniques 2018;64:203–10.
25. Toth M, Fridman R.Assessment of gelatinases (MMP-2 and MMP-9 by gelatin zymography. Methods Mol Med 2001;57:163–74.
26. Ren Z, Chen J, Khalil RA. Zymography as a research tool in the study of matrix metalloproteinase inhibitors. Methods Mol Biol 2017;1626:79–102.
27. Lee C, Scherer SW.The clinical context of copy number variation in the human genome. Expert Rev Mol Med 2010;12:e8.
28. Wang S, Sun W, Zhao Y, McEachern D, Meaux I, Barriere C, et al. SAR405838: an optimized inhibitor of MDM2-p53 interaction that induces complete and durable tumor regression. Cancer Res 2014;74:5855–65.
29. Lobb RJ, Lima LG, Moller A. Exosomes: key mediators of metastasis and pre-metastatic niche formation. Semin Cell Develop Biol 2017;67:3–10.
30. Kosaka N, Iguchi H, Yoshioka Y, Takeshita F, Matsuki Y, Ochiya T. Secretory mechanisms and intercellular transfer of microRNAs in living cells. J Biol Chem 2010;285:17442–52.
31. Aleckovic M, Kang Y.Regulation of cancer metastasis by cell-free miRNAs. Biochim Biophys Acta 2015;1855:24–42.
32. Chin AR, Wang SE.Cancer tills the premetastatic field: mechanistic basis and clinical implications. Clin Cancer Res 2016;22:3725–33.
33. Thuma F, Zoller M.Outsmart tumor exosomes to steal the cancer initiating cell its niche. Semin Cancer Biol 2014;28:39–50.
34. Rayburn E, Zhang R, He J, Wang H. MDM2 and human malignancies: expression, clinical pathology, prognostic markers, and implications for chemotherapy. Curr Cancer Drug Targets 2005;5:27–41.
35. Murphy G, Crabbe T. Gelatinases A and B. Methods in enzymology1995;248:470–84.
36. Stetler-Stevenson WG.Type IV collagenases in tumor invasion and metastasis. Cancer Metastasis Rev 1990;9:289–303.
37. Iivanainen E, Kahari VM, Heino J, Elenius K. Endothelial cell-matrix interactions. Microsc Res Tech 2003;60:13–22.
38. Shay G, Lynch CC, Fingleton B. Moving targets: Emerging roles for MMPs in cancer progression and metastasis. Matrix Biol 2015;44–46:200–6.
39. Bates AL, Pickup MW, Hallett MA, Dozier EA, Thomas S, Fingleton B. Stromal matrix metalloproteinase 2 regulates collagen expression and promotes the outgrowth of experimental metastases. J Pathol 2015;235:773–83.
40. Deryugina EI, Quigley JP. Matrix metalloproteinases and tumor metastasis. Cancer Metastasis Rev 2006;25:9–34.
41. Donadio AC, Durand S, Remedi MM, Frede S, Ceschin DG, Genti-Raimondi S, et al. Evaluation of stromal metalloproteinases and vascular endothelial growth factors in a spontaneous metastasis model. Exp Mol Pathol 2005;79:259–64.
42. Mendes O, Kim HT, Lungu G, Stoica G. MMP2 role in breast cancer brain metastasis development and its regulation by TIMP2 and ERK1/2. Clin Exp Metast 2007;24:341–51.

43. Yang HK, Jeong KC, Kim YK, Jung ST. Role of matrix metalloproteinase (MMP) 2 and MMP-9 in soft tissue sarcoma. Clin Orthoped Surg 2014;6: 443–54.
44. Yao Z, Yuan T, Wang H, Yao S, Zhao Y, Liu Y, et al. MMP-2 together with MMP-9 overexpression correlated with lymph node metastasis and poor prognosis in early gastric carcinoma. Tumour Biol 2017;39: 1010428317700411.
45. Pazzaglia L, Ponticelli F, Magagnoli G, Magagnoli G, Gamberi G, Ragazzini P, et al. Activation of metalloproteinases-2 and -9 by interleukin-1alpha in S100A4-positive liposarcoma cell line: correlation with cell invasiveness. Anticancer Res 2004;24:967–72.
46. Benassi MS, Gamberi G, Magagnoli G, Molendini L, Ragazzini P, Merli M, et al. Metalloproteinase expression and prognosis in soft tissue sarcomas. Ann Oncol 2001;12:75–80.
47. Bradbury R, Jiang WG, Cui YX. MDM2 and PSMA play inhibitory roles in metastatic breast cancer cells through regulation of matrix metalloproteinases. Anticancer Res 2016;36: 1143–51.